

# Thermodynamic Performance of Three-Terminal Hybrid Quantum Dot Thermoelectric Devices \*

Zhi-Cheng Shi(施志成), Jing Fu(符婧), Wei-Feng Qin(秦伟锋), Ji-Zhou He(何济洲)\*\*

Department of Physics, Nanchang University, Nanchang 330031

(Received 22 March 2017)

We propose four different models of three-terminal quantum dot thermoelectric devices. From general thermodynamic laws, we examine the reversible efficiencies of the four different models. Based on the master equation, the expressions for the efficiency and power output are derived and the corresponding working regions are determined. Moreover, we particularly analyze the performance of a three-terminal hybrid quantum dot refrigerator. The performance characteristic curves and the optimal performance parameters are obtained. Finally, we discuss the influence of the nonradiative effects on the optimal performance parameters in detail.

PACS: 05.70.-a, 73.50.Lw, 73.63.Kv, 85.80.Fi

DOI: 10.1088/0256-307X/34/11/110501

Recently, various three-terminal thermoelectric devices and processes have been proposed, where the electrons interchange energy with a boson or Fermi reservoir, e.g., photons, phonons, electron-hole excitations, electrons or magnons. The boson or Fermi reservoir coupled to the electron system represents the third terminal, making the setup a three-terminal one.<sup>[1–19]</sup> Compared with two-terminal thermoelectric devices, three-terminal thermoelectric ones can separate electric and heat currents. In this study, we propose four different models of the three-terminal quantum dot thermoelectric devices and define various efficiencies (or, equivalently, coefficients of performance). As an example, we analyze the thermodynamic performance characteristics and optimal performance of a three-terminal quantum dot hybrid thermoelectric refrigerator. The influence of the nonradiative effect on the optimal performance parameters is discussed in detail.

The three-terminal quantum dot thermoelectric device we consider is illustrated in Fig. 1. The two coupled single-level quantum dots with energy levels  $\varepsilon_L$  and  $\varepsilon_R$  ( $\varepsilon_L < \varepsilon_R$ ) are connected with the two electronic terminals at different temperatures  $T_L$  and  $T_R$ , respectively. The single energy level  $\varepsilon_L$  ( $\varepsilon_R$ ) is near the Fermi level of the left (right) electronic terminal, and we define the energy level difference  $\varepsilon_g = \varepsilon_R - \varepsilon_L$ . The left (right) quantum dot with energy level  $\varepsilon_L$  ( $\varepsilon_R$ ) can only exchange electrons with the left (right) terminal, respectively. The left and right terminals are connected by an external circuit (an applied bias voltage  $\Delta V = (\mu_R - \mu_L)/q$  or a load, where  $q$  is the charge of an electron). We suppose that the Coulomb interactions prevent two electrons from being present at the same time. Thus the single energy level  $\varepsilon_L$  ( $\varepsilon_R$ ) can be occupied only by zero or one electron with respective probabilities  $p_i$  with  $i \in \{0, L, R\}$ . The left (right) quantum dot is coupled by two possible mechanisms. The first is due to the incoming photon (thermal terminal with temperature kept at  $T_T$ ) radiation at the resonant energy of  $\varepsilon_g = h\nu$ . The second is due to nonradiative processes at the same resonant transition. The relationship between the temperatures of the three terminals satisfies  $T_L < T_R < T_T$ . Driven by

thermal photons, electrons can be transmitted from the left terminal to the right terminal via the left and right quantum dots and come back to the left terminal through an external circuit, forming a net circulation of electrons. Such a three-terminal quantum dot thermoelectric device can be designed to operate in four different scenarios (models), as shown in Figs. 1(a)–1(d).

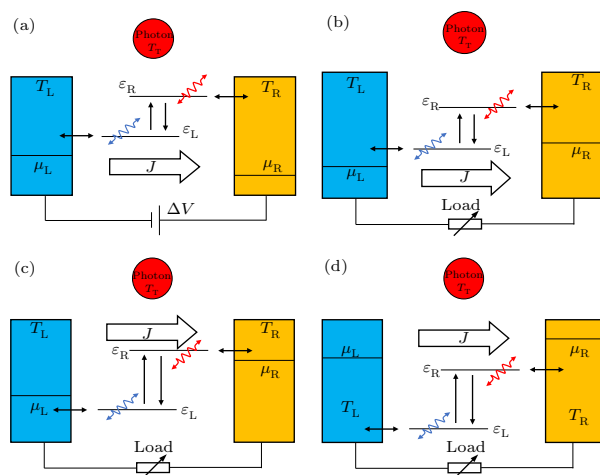


**Fig. 1.** The schematic diagram of three-terminal quantum dot thermoelectric devices in four different scenarios. The dark arrows show the different allowed electron transitions. Transitions between the left and the right energy levels induced by thermal photons, and nonradiative processes are indicated by an upper curly red arrow and a lower curly blue arrow, respectively. The overall electron current through the device is shown by the hollow arrow with  $J$ . The left and right electronic terminals are connected by a load or bias voltage.

The operating principle of various scenarios is described as follows: (a) Three-terminal hybrid thermoelectric refrigerator: it is a ‘double driving’ refrigerator model. The ‘double driving’ comprises the heat  $\dot{Q}_T$  from the thermal terminal and the electric power  $-P_E$  supplied by the applied bias voltage, taking heat  $\dot{Q}_L$  from the left terminal and dumping heat  $-\dot{Q}_R$  into the right terminal. Thus  $\dot{Q}_L$  is the cooling power, and

\*Supported by the National Natural Science Foundation of China under Grant No 11365015.

\*\*Corresponding author. Email: hjzhou@ncu.edu.cn

© 2017 Chinese Physical Society and IOP Publishing Ltd

the COP of the refrigerator is defined as

$$\eta_{(a)} = \begin{cases} \dot{Q}_L/(-P_E), & \Delta V \neq 0, \\ \dot{Q}_L/\dot{Q}_T, & \Delta V = 0. \end{cases} \quad (1)$$

For a reversible process, the entropy production rate is

$$\dot{S} = -\frac{\dot{Q}_T}{T_T} - \frac{\dot{Q}_L}{T_L} - \frac{\dot{Q}_R}{T_R} = 0. \quad (2)$$

Combining the energy conservation formula

$$\dot{Q}_L + \dot{Q}_T + \dot{Q}_R - P_E = 0, \quad (3)$$

the corresponding reversible COP is obtained as follows:

$$\eta_{(a)}^{\text{rev}} = \frac{\dot{Q}_L/\dot{Q}_T}{1 - T_R/T_T - (\dot{Q}_L/\dot{Q}_T)(T_R/T_L - 1)}. \quad (4)$$

When the applied bias voltage is zero, the reversible COP is  $(1 - \frac{T_R}{T_T})\frac{T_L}{T_R - T_L}$ .<sup>[18]</sup>

(b) Three-terminal hybrid thermoelectric heat engine: it absorbs the invested heat  $\dot{Q}_T$  from the thermal terminal and the heat  $\dot{Q}_L$  from the left terminal, releases heat  $-\dot{Q}_R$  to the right terminal, and produces the electric power  $P_E$ . The efficiency is defined as<sup>[19]</sup>

$$\eta_{(b)} = \frac{P_E}{\dot{Q}_L + \dot{Q}_T}. \quad (5)$$

For a reversible process, using Eqs. (2), (3) and (5), we obtain the reversible efficiency

$$\eta_{(b)}^{\text{rev}} = \left(1 - \frac{T_R}{T_T}\right) - \frac{T_R}{T_T} \frac{T_T/T_L - 1}{1 + \dot{Q}_T/\dot{Q}_L}. \quad (6)$$

In particular, when  $\dot{Q}_L = 0$ , the reversible efficiency is reduced to

$$\eta_{(b)}^{\text{rev}} = 1 - \frac{T_R}{T_T}, \quad (7)$$

which is the Carnot efficiency of the two-terminal case.

(c) General three-terminal thermoelectric heat engine: it absorbs heat  $\dot{Q}_T$  from the thermal terminal, releases heat  $-\dot{Q}_L$  to the left electronic terminal and heat  $-\dot{Q}_R$  to the right electronic terminal, and produces the electric power  $P_E$ . The efficiency is defined as<sup>[19]</sup>

$$\eta_{(c)} = P_E/\dot{Q}_T. \quad (8)$$

For a reversible process, using Eqs. (2), (3) and (8) we can obtain the corresponding reversible efficiency

$$\begin{aligned} \eta_{(c)}^{\text{rev}} &= \left(1 - \frac{T_R}{T_T}\right) + \frac{\dot{Q}_L}{\dot{Q}_T} \left(1 - \frac{T_R}{T_L}\right) \\ &= \left(1 - \frac{T_L}{T_T}\right) + \frac{\dot{Q}_R}{\dot{Q}_T} \left(1 - \frac{T_L}{T_R}\right). \end{aligned} \quad (9)$$

It is obvious that  $\dot{Q}_L/\dot{Q}_T \leq 0$  and  $\dot{Q}_R/\dot{Q}_T \leq 0$ , thus we have

$$1 - \frac{T_R}{T_T} \leq \eta_{(c)}^{\text{rev}} \leq 1 - \frac{T_L}{T_T}. \quad (10)$$

Notice that, when  $\dot{Q}_L = 0$  or  $\dot{Q}_R = 0$ , the three-terminal model degenerates to a two-terminal one, and the corresponding Carnot efficiencies  $1 - T_R/T_T$  and  $1 - T_L/T_T$  are obtained. In particular, when  $T_L = T_R = T$ , this model is similar to the ‘solar cell’,<sup>[14]</sup> and the reversible efficiency is the Carnot value  $\eta_{(c)}^{\text{rev}} = 1 - T/T_T$  like a two-terminal one.

(d) Another kind of general three-terminal thermoelectric heat engine: it absorbs the invested heat  $\dot{Q}_T$  from the thermal terminal and the heat  $\dot{Q}_R$  from the right terminal, releases heat  $-\dot{Q}_L$  to the left terminal, and produces the electric power  $P_E$ . The efficiency is defined as

$$\eta_{(d)} = P_E/(\dot{Q}_T + \dot{Q}_R). \quad (11)$$

For the reversible process, using Eqs. (2), (3) and (11), similarly we obtain the reversible efficiency<sup>[19]</sup>

$$\eta_{(d)}^{\text{rev}} = \left(1 - \frac{T_L}{T_T}\right) - \frac{T_L}{T_T} \frac{T_T/T_R - 1}{1 + \dot{Q}_T/\dot{Q}_R}. \quad (12)$$

In this case,  $\dot{Q}_T/\dot{Q}_R$  is bounded in  $[0, +\infty)$ , in the limits  $\dot{Q}_T/\dot{Q}_R = 0$  ( $\dot{Q}_T = 0$ ) and  $\dot{Q}_T/\dot{Q}_R \rightarrow \infty$  ( $\dot{Q}_R = 0$ ), Eq. (12) is bounded in

$$1 - \frac{T_L}{T_R} \leq \eta_{(d)}^{\text{rev}} \leq 1 - \frac{T_L}{T_T}. \quad (13)$$

We also find that the lower bound and the upper bound of  $\eta_{(d)}^{\text{rev}}$  are the Carnot efficiencies for the two-terminal ones. In particular, when  $T_R = T_T = T$ , the reversible efficiency is also the Carnot value  $\eta_{(d)}^{\text{rev}} = 1 - T_L/T_T$ .

The dynamics of the left and right quantum dots is described using the master equation formulation for driven open systems. The evolution of the probabilities  $p_0$ ,  $p_L$ , and  $p_R$  to find no electron or one electron in energy level  $\varepsilon_L$  or  $\varepsilon_R$ , respectively, with time is given by<sup>[14]</sup>

$$\begin{aligned} \begin{bmatrix} \dot{p}_0 \\ \dot{p}_L \\ \dot{p}_R \end{bmatrix} &= \begin{bmatrix} -k_{0L} - k_{0R} & k_{L0} & k_{R0} \\ k_{0L} & -k_{L0} - k_{LR} & k_{RL} \\ k_{0R} & k_{LR} & -k_{R0} - k_{RL} \end{bmatrix} \\ &\cdot \begin{bmatrix} p_0 \\ p_L \\ p_R \end{bmatrix}. \end{aligned} \quad (14)$$

At the steady state, i.e.,  $\dot{p}_0 = \dot{p}_L = \dot{p}_R = 0$ , and the probabilities meet  $p_0 + p_L + p_R = 1$ . The occupation probabilities of each state are derived as

$$p_0 = \frac{k_{L0}k_{R0} + k_{LR}k_{R0} + k_{L0}k_{RL}}{\Omega}, \quad (15a)$$

$$p_L = \frac{k_{0L}k_{R0} + k_{0L}k_{RL} + k_{0R}k_{RL}}{\Omega}, \quad (15b)$$

$$p_R = \frac{k_{L0}k_{0R} + k_{LR}k_{0L} + k_{LR}k_{0R}}{\Omega}, \quad (15c)$$

where  $\Omega = k_{0R}k_{L0} + k_{0L}k_{LR} + k_{0R}k_{LR} + k_{0L}k_{R0} + k_{L0}k_{R0} + k_{LR}k_{R0} + k_{0L}k_{RL} + k_{0R}k_{RL} + k_{L0}k_{RL}$  is the normalization factor that ensures the sum of probabilities to be equal to unity,  $k_{ij}$  ( $i, j = 0, L, R$ ) is the transition rate from state  $i$  to state  $j$ . The rates describing the exchange of electrons with the electronic terminals are given by

$$k_{0L} = \Gamma_L f(x_L), \quad (16a)$$

$$k_{L0} = \Gamma_L [1 - f(x_L)], \quad (16b)$$

$$k_{0R} = \Gamma_R f(x_R), \quad (16c)$$

$$k_{R0} = \Gamma_R [1 - f(x_R)], \quad (16d)$$

where  $f(x) = 1/[\exp(x) + 1]$  is the Fermi distribution,  $x_L = (\varepsilon_L - \mu_L)/k_B T_L$  and  $x_R = (\varepsilon_R - \mu_R)/k_B T_R$  are the scaled energies,  $k_B$  is the Boltzmann constant,  $\Gamma_L$  and  $\Gamma_R$  are the bare tunneling rates between energy level  $\varepsilon_i$  ( $i = L, R$ ) and the corresponding electronic terminal. The rates describing the transitions between energy levels due to photons from the thermal terminal (T) and to nonradiative (nr) effects are given by

$$k_{LR} = \Gamma_T n(x_T) + \Gamma_{nr} n(x_{gL}), \quad (17a)$$

$$k_{RL} = \Gamma_T [1 + n(x_T)] + \Gamma_{nr} [1 + n(x_{gR})], \quad (17b)$$

where  $n(x) = 1/[\exp(x) - 1]$  is the Bose-Einstein distribution with the scaled energy  $x_T = \varepsilon_g/k_B T_T$ ,  $x_{gL} = \varepsilon_g/k_B T_L$  and  $x_{gR} = \varepsilon_g/k_B T_R$ ,  $\Gamma_T$  is the proportional constant of the photon radiative processes, and  $\Gamma_{nr}$  is the proportional constant of the nonradiative processes. Notice that  $\Gamma_{nr}$  indicates the strength of nonradiative effect.

At the steady state, the electron current entering the left quantum dot from the left terminal is equal to the electron current from right quantum dot to right terminal. It can be written as

$$J = k_{0L}p_0 - k_{L0}p_L = k_{R0}p_R - k_{0R}p_0. \quad (18)$$

This current can be decomposed as  $J = J_T + J_{nr}$ , with  $J_T$  and  $J_{nr}$  being the contributions to the current due to the interaction with the thermal photons and the nonradiative processes, respectively,

$$J_T = \Gamma_T n(x_T)p_L - \Gamma_T [1 + n(x_T)]p_R, \quad (19)$$

$$J_{nr} = \Gamma_{nr} n(x_{gL})p_L - \Gamma_{nr} [1 + n(x_{gR})]p_R. \quad (20)$$

The motion of the electrons between the electronic terminals and the system gives rise to an associated heat exchange. According to the fundamental equation of thermodynamics for an open system at constant volume and pressure, we can obtain the associated heat current flowing from the electronic terminals at the steady state, which are given by

$$\dot{Q}_L = J(\varepsilon_L - \mu_L), \quad (21)$$

$$\dot{Q}_R = -J(\varepsilon_R - \mu_R). \quad (22)$$

The net heat current coming from the thermal photon terminal is

$$\dot{Q}_T = J_T \varepsilon_g, \quad (23)$$

whereas the heat current due to the nonradiative processes is

$$\dot{Q}_{nr} = J_{nr} \varepsilon_g. \quad (24)$$

The electric output power is expressed as

$$P_E = J(\mu_R - \mu_L). \quad (25)$$

We can verify that  $\dot{Q}_L + \dot{Q}_R + \dot{Q}_T + \dot{Q}_{nr} - P_E = 0$ . This energy conservation formula is suitable for the above four different models. Thus we can rewrite the expressions for the efficiency or the COP of each model as

$$\eta_{(a)} = \begin{cases} \frac{\dot{Q}_L}{-P_E} = \frac{\varepsilon_L - \mu_L}{\mu_L - \mu_R}, & \Delta V \neq 0, \\ \frac{\dot{Q}_L}{\dot{Q}_T} = \frac{J(\varepsilon_L - \mu_L)}{J_T \varepsilon_g}, & \Delta V = 0, \end{cases} \quad (26a)$$

$$\eta_{(b)} = \frac{P_E}{\dot{Q}_L + \dot{Q}_T} = \frac{J(\mu_R - \mu_L)}{J(\varepsilon_L - \mu_L) + J_T \varepsilon_g}, \quad (26b)$$

$$\eta_{(c)} = \frac{P_E}{\dot{Q}_T} = \frac{J(\mu_R - \mu_L)}{J_T \varepsilon_g}, \quad (26c)$$

$$\eta_{(d)} = \frac{P_E}{\dot{Q}_T + \dot{Q}_R} = \frac{J(\mu_R - \mu_L)}{J_T \varepsilon_g - J(\varepsilon_R - \mu_R)}. \quad (26d)$$

It is found from Eqs. (21)–(26) that the performance parameters of the device (e.g., electric output power, efficiency or COP) are the functions of the positions of energy level  $\varepsilon_L$  and  $\varepsilon_R$  of two quantum dots, the temperatures  $T_L$ ,  $T_R$  and  $T_T$ , the chemical potentials  $\mu_L$  and  $\mu_R$  of two electronic terminals, the bias voltage  $\Delta V$ , the strength of nonradiative effect  $\Gamma_{nr}$ , and the bare tunneling rates  $\Gamma_L$ ,  $\Gamma_R$  and  $\Gamma_T$ .

Since the three-terminal quantum dot thermoelectric device can operate in four different models, one may obtain the corresponding working regions by deciding the signs of the four thermodynamic parameters  $\dot{Q}_L$ ,  $\dot{Q}_R$ ,  $\dot{Q}_T$  and  $P_E$ . In model (a):  $\dot{Q}_T > 0$ ,  $\dot{Q}_L > 0$ ,  $\dot{Q}_R < 0$ , and  $P_E < 0$ ; in model (b):  $\dot{Q}_T > 0$ ,  $\dot{Q}_L > 0$ ,  $\dot{Q}_R < 0$ , and  $P_E > 0$ ; in model (c):  $\dot{Q}_T > 0$ ,  $\dot{Q}_L < 0$ ,  $\dot{Q}_R < 0$ , and  $P_E > 0$ ; and in model (d):  $\dot{Q}_T > 0$ ,  $\dot{Q}_L < 0$ ,  $\dot{Q}_R > 0$ , and  $P_E > 0$ .

When the nonradiative effect  $\Gamma_{nr}$  is not taken into account, we have  $J_T = J$  and  $\dot{Q}_{nr} = 0$ . The overall entropy production rate is given by

$$\dot{S} = -J \left( \frac{\varepsilon_L - \mu_L}{T_L} - \frac{\varepsilon_R - \mu_R}{T_R} + \frac{\varepsilon_g}{T_T} \right). \quad (27)$$

According to the principle of entropy increase, i.e.,  $\dot{S} \geq 0$ , we find  $J \geq 0$  corresponding to the region

$$\frac{x}{T_L} - \frac{y}{T_R} + \frac{\varepsilon_g}{T_T} \leq 0, \quad (28)$$

where  $x \equiv \varepsilon_L - \mu_L$  and  $y \equiv \varepsilon_R - \mu_R$  are the relative positions of the two energy levels in relation to the chemical potential of left (right) electronic terminal. Thus the difference of chemical potential is

$$\mu_L - \mu_R = y - x - \varepsilon_g. \quad (29)$$

The inequality (28) and Eq. (29) play an important role in deciding the signs of  $\dot{Q}_L$ ,  $\dot{Q}_R$ ,  $\dot{Q}_T$  and  $P_E$ .

Interestingly, when the inequality (28) takes the equal sign, i.e.,  $\dot{S} = 0$ , associating with Eqs. (15)–(18), we verify that  $J = 0$ . This means that the electrons can reversibly transfer between the two electronic terminals and the quantum dots. We also derive the relationship between efficiency and entropy production rate

$$\eta_{(a)} = \frac{\alpha}{1 - T_R/T_T - \alpha(T_R/T_L - 1) - T_R\dot{S}/\dot{Q}_T}, \quad (30a)$$

$$\eta_{(b)} = 1 - \frac{T_R}{T_T} - \frac{T_R}{T_T} \frac{T_T/T_L - 1}{1 + \dot{Q}_T/\dot{Q}_L} - \frac{T_R\dot{S}}{\dot{Q}_L + \dot{Q}_T}, \quad (30b)$$

$$\begin{aligned} \eta_{(c)} &= 1 - \frac{T_R}{T_T} + \frac{\dot{Q}_L}{\dot{Q}_T} \left(1 - \frac{T_R}{T_L}\right) - \frac{T_R\dot{S}}{\dot{Q}_T} \\ &= 1 - \frac{T_L}{T_T} + \left(1 - \frac{T_L}{T_R}\right) \frac{\dot{Q}_R}{\dot{Q}_T} - \frac{T_L\dot{S}}{\dot{Q}_T}, \end{aligned} \quad (30c)$$

$$\eta_{(d)} = 1 - \frac{T_L}{T_T} - \frac{T_L}{T_T} \frac{T_T/T_R - 1}{1 + \dot{Q}_T/\dot{Q}_R} - \frac{T_L\dot{S}}{\dot{Q}_R + \dot{Q}_T}. \quad (30d)$$

According to Eqs. (21)–(23) and (25), we obtain the corresponding working regions of the four different models when  $\Gamma_{nr} = 0$ , as shown in Fig. 2. In the analytical calculation, it is set that  $T_L = 4$  K,  $T_R = 8$  K,  $T_T = 16$  K,  $\varepsilon_g/k_B = 6$  K,  $\Gamma_{nr} = 0$ , and  $\Gamma_T = \Gamma_L = \Gamma_R = \Gamma$ . It is seen from Fig. 2 that by tuning the relative positions of the two energy levels, the device can operate in four different models at other related parameters given.

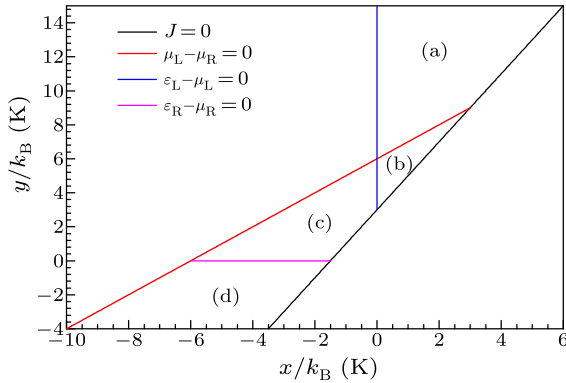


**Fig. 2.** The corresponding working regions of the four different models.

For convenience and uniformity, we introduce the total power output  $P$  for each model, i.e.,

$$P = \begin{cases} \dot{Q}_L, & \text{model (a),} \\ P_E, & \text{models (b), (c) and (d).} \end{cases} \quad (31)$$

Using Eqs. (21)–(26) and (30), we plot the three-dimensional (3D) projection graph of the total power output  $P$  and the efficiency  $\eta$  varying with the relative positions of the two energy levels  $x$  and  $y$  at different nonradiative effects  $\Gamma_{nr}$ , as shown in Figs. 3 and 4. It is seen that when the nonradiative effects do not exist ( $\Gamma_{nr} = 0$ ), the working regions will be in good agreement with that in Fig. 2. When the nonradiative effects exist, the working regions can only be numerically calculated. As the nonradiative effects increase, the corresponding working regions diminish

gradually. Some positive values in the working regions can be decreased to zero or negative, and hence the working regions diminish gradually as the nonradiative effects increase. Since the corresponding working regions for models (b) and (c) are finite, we can infer that these two regions will vanish at some values of  $\Gamma_{nr}$ . Both the total output power  $P$  and the efficiency (or COP)  $\eta$  decrease as the nonradiative effects  $\Gamma_{nr}$  increase. When the nonradiative effects do not exist, the efficiency  $\eta$  monotonously varies with  $x$  or  $y$  when the other of them are given, and the maximum efficiency  $\eta_{max}$  should lie on the line for  $J = 0$  since the device can reversibly operate in this case. Particularly in region (a), i.e., the device works as a ‘double driving’ refrigerator, the contour for  $\mu_L - \mu_R$  (white dashed line) becomes longer as its value increases. This means that as the applied bias voltage  $\Delta V$  increases, the working region will increase, and more cooling power  $\dot{Q}_L$  ( $P$ ) can be obtained. These are the advantages of the double driving refrigerator.

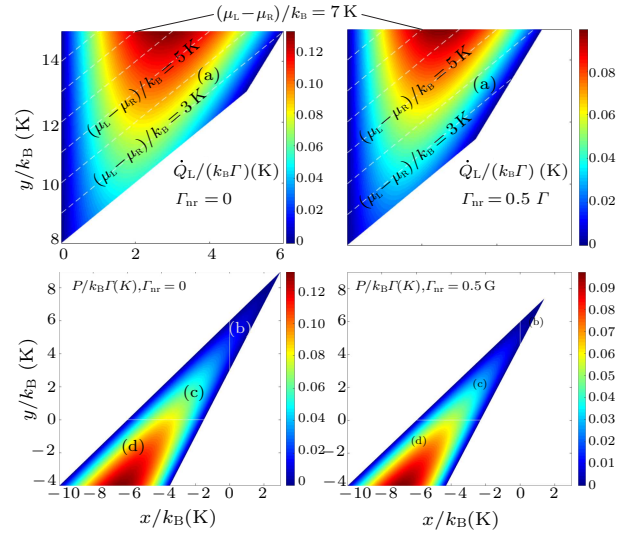


**Fig. 3.** The 3D projection graph of the total output power  $P$  varying with  $x$  and  $y$  at different nonradiative effects  $\Gamma_{nr}$ .

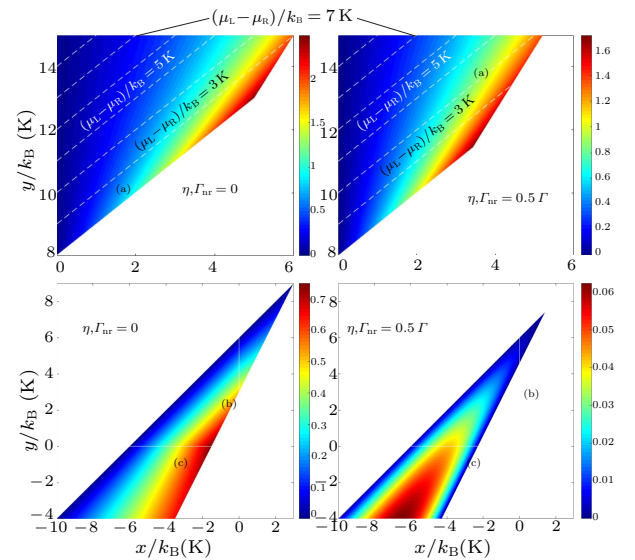


**Fig. 4.** The 3D projection graph of the efficiency  $\eta$  varying with  $x$  and  $y$  at different nonradiative effects  $\Gamma_{nr}$ .

Using Eqs. (22)–(27a), we plot the performance characteristic curves of the cooling rate  $\dot{Q}_L$  versus COP  $\eta$  at different nonradiative effects  $\Gamma_{nr}$  and applied bias voltage when the device works as a ‘double driving’ refrigerator, as shown in Fig. 5. It can be seen from Fig. 5 that, when the applied bias voltage is zero, the performance characteristic curve for  $\Gamma_{nr} = 0.1\Gamma$  is a closed loop-shaped one, while these curves are open-shaped when  $\Gamma_{nr} = 0$  or the applied bias voltage is nonzero. The performance characteristic curves for  $\Delta V > 0$  present a special point: the maximum cooling rate point ( $\eta_{QL}, \dot{Q}_{L,max}$ ). As the nonradiative effects  $\Gamma_{nr}$  increase, both the maximum cooling power  $\dot{Q}_{L,max}$  and the corresponding COP  $\eta_{QL}$  decrease. The optimal thermodynamic performance parameters at the maximum cooling rate can be numerically calculated.

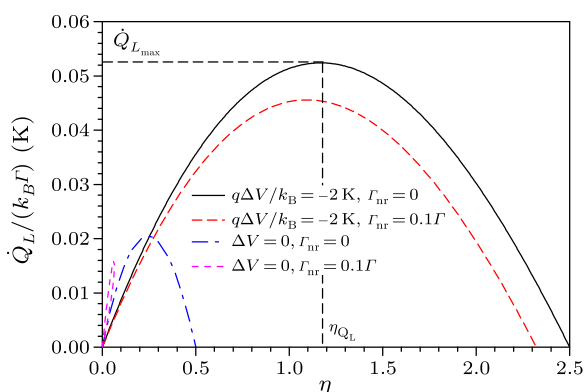


**Fig. 5.** The performance characteristic curves of the cooling power versus the coefficient of performance at different nonradiative effects  $\Gamma_{nr}$  and applied bias voltages.

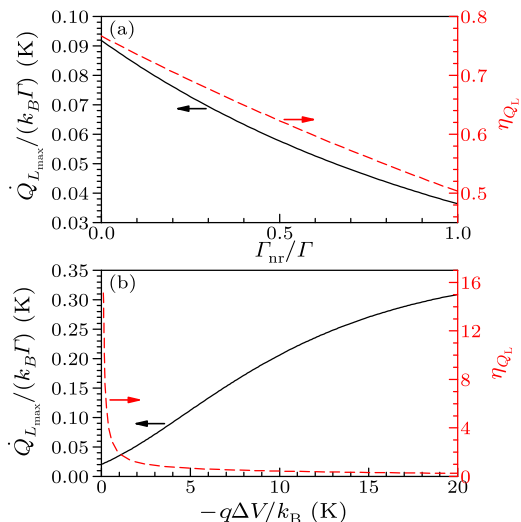


**Fig. 6.** The curves of the maximum cooling rate and the corresponding COP versus the nonradiative effects  $\Gamma_{nr}$  at given  $-q\Delta V/k_B = 4$  K and versus the applied bias voltage  $\Delta V$  when the nonradiative effects do not exist.

Using Eqs. (22) and (27a) and the extremal conditions

$$\frac{\partial \dot{Q}_L}{\partial x} = 0, \quad (32)$$

we can numerically calculate the maximum cooling rate  $\dot{Q}_{L,max}$  and the corresponding COP  $\eta_{QL}$ . The curves of the two optimal performance parameters versus the nonradiative effects  $\Gamma_{nr}$  or the applied bias voltage  $\Delta V$  are plotted in Fig. 6. It can be seen that both the maximum cooling rate  $\dot{Q}_{L,max}$  and the corresponding COP  $\eta_{QL}$  monotonously decrease as the nonradiative effects  $\Gamma_{nr}$  increase. Thus in the actual maximum cooling rate design one should minimize the nonradiative effects  $\Gamma_{nr}$  as largely as possible. As the applied bias voltage  $\Delta V$  increases, the maximum cooling rate  $\dot{Q}_{L,max}$  increases monotonously while the corresponding COP  $\eta_{QL}$  monotonously decreases.

The main results obtained are as follows: (1) as the nonradiative effects  $\Gamma_{nr}$  increase, the corresponding working regions diminish gradually and both the total output power and the efficiency also decrease. (2) For a hybrid thermoelectric refrigerator, as the applied bias voltage increases, the working region will increase, more cooling power can be obtained. (3) The optimal performance of the hybrid thermoelectric refrigerator is analyzed and the influence of the nonradiative effect  $\Gamma_{nr}$  and applied bias voltage  $\Delta V$  on the optimal performance parameters is revealed. The results obtained here can provide some theoretical guidelines for the design and operation of practical quantum dot thermoelectric devices.

## References

- [1] Sothmann B, Sanchez R and Jordan A N 2015 *Nanotechnology* **26** 032001
- [2] Edwards H L, Niu Q and De Lozanne A L 1993 *Appl. Phys. Lett.* **63** 1815
- [3] Edwards H L, Niu Q, Georgakis G A and De Lozanne A L 1995 *Phys. Rev. B* **52** 5714
- [4] Prance J R, Smith C G, Griffiths J P, Chorley S J, Anderson D A, Jones G A C, Farrer I and Ritchie D A 2009 *Phys. Rev. Lett.* **102** 146602
- [5] Jordan A N, Sothmann B, Sanchez R and Büttiker M 2013 *Phys. Rev. B* **87** 075312
- [6] Sothmann B, Sanchez R, Jordan A N and Büttiker M 2013 *New J. Phys.* **15** 095021
- [7] Su S H, Zhang Y C, Chen J C and Shih T M 2016 *Sci. Rep.* **6** 21425
- [8] Su G Z, Zhang Y C, Cai L, Su S H and Chen J C 2015 *Energy* **90** 1842
- [9] Su H, Shi Z C and He J Z 2015 *Chin. Phys. Lett.* **32** 100501
- [10] Jiang J H, Entin-Wohlman O and Imry Y 2012 *Phys. Rev. B* **85** 075412
- [11] Jiang J H 2014 *J. Appl. Phys.* **116** 194303
- [12] Sanchez R and Büttiker M 2011 *Phys. Rev. B* **83** 085428
- [13] Zhang Y C, Lin G X and Chen J C 2015 *Phys. Rev. E* **91** 052118
- [14] Rутten B, Esposito M and Cleuren B 2009 *Phys. Rev. B* **80** 235122
- [15] Cleuren B, Rутten B and van den Broeck C 2012 *Phys. Rev. Lett.* **108** 120603
- [16] Shi Z C, He J Z and Xiao Y L 2015 *Sci. Sin-Phys. Mech. Astron.* **45** 050502 (in Chinese)
- [17] Li C, Zhang Y C, Wang J H and He J Z 2013 *Phys. Rev. E* **88** 062120
- [18] Entin-Wohlman O, Imry Y and Aharony A 2015 *Phys. Rev. B* **91** 054302
- [19] Mazza F, Bosisio R, Benenti G, Giovannetti V, Fazio R and Taddei F 2014 *New J. Phys.* **16** 085001